J|A|C|S
ARTICLES
Published on Web 05/25/2006

Quantitative Imaging of Protein Adsorption on Patterned Organic Thin-Film Arrays Using Secondary Electron Emission

Nathan H. Mack, Rui Dong, and Ralph G. Nuzzo*

Contribution from the Department of Chemistry, University of Illinois at Urbana-Champaign, 600 South Mathews Avenue, Urbana, Illinois 61801

Received January 23, 2006; E-mail: r-nuzzo@uiuc.edu

Abstract: Secondary electron emission is developed as a means to quantify and image protein binding to Au surfaces modified with patterned organic thin-film arrays. Alkane thiols were patterned via microcontact printing on gold, and their effects on the secondary electron (SE) yield of the surface, systematically quantified. We show that a self-assembled monolayer (SAM) of hexadecane thiol significantly increases the SE yield over the native gold surface, a yield that increases as a function of alkane chain length (C_8−C_{16}). This effect is linearly correlated with the surface potentials and wetting properties of these SAMs. Surface layers comprised of poly(ethylene glycol) (PEG) grafted polyacrylamide polymers behave differently, affecting the SE yield by attenuation according to the polymer thickness. These results demonstrate the relative contributions of factors related to the adsorbate molecular structures that serve to strongly mediate the SE yield, providing a foundation for exploiting them as a quantitative electron imaging probe. The latter capability is demonstrated using a model microfluidic assay in which a series of proteins was spatially addressed to a SAM-based pixel array. The gray scale contrasts seen with protein adsorption are directly correlated with both protein molecular weight and mass coverage. These methods are used in two model protein assay experiments: (1) the measurement of the concentration dependent adsorption isotherm for a model protein (fibrinogen); and (2) the selective recognition of a biotinylated protein layer by avidin. These results demonstrate a unique approach to imaging protein binding processes on surfaces with both high analytical and spatial sensitivity.

Introduction

Recent work in the area of biotechnology has come to increasingly focus on the control and manipulation of biological cells in culture on surfaces as one means for studying the nature of complex chemical signaling interactions.[1−3] This type of research requires capacities for exerting control of the chemistry at the cell-surface interface and often uses adsorbed proteins in diverse, and frequently patterned, forms.[4] Soft-lithography and functional self-assembled monolayers (SAMs) have proven to be especially useful tools for such studies, ones that provide diverse forms of modified surfaces that can be used to promote cell adhesion and growth.[5]

SAMs of alkane (and other organic) thiols have been extensively studied as model systems for protein adsorption due to the chemically well-defined nature of the surfaces they provide and the broad spectrum of surface-chemical properties they enable.[6] For example, oligo-ethyleneglycol terminated alkane thiols have been shown to generally resist nonspecific protein adsorption, while methyl terminated alkane thiols tend to strongly promote such binding.[7] The mechanisms that control such behaviors have been much discussed and remain highly controversial.[8] This work has served to stimulate interest in SAMs as tools for discovery in biology and inspired research seeking to provide means through which they can be used to rapidly detect the adsorption of multiple proteins onto surfaces functionalized in array based forms. The present work addresses itself to this latter interest, extending earlier work that examined adsorption processes involving SAMs using SEM.[9]

Numerous techniques are presently used to detect protein surface binding events. Each technique, however, has inherent limitations that reduce their potential for high throughput protein screening. For example, fluorescence microscopies require spectroscopic labeling which can introduce protein affinity artifacts, as well as increase the complexity and cost of sample preparation.[10] Scanning ellipsometry and atomic force microscopy (AFM) offer exceptional sensitivity to surface bound analytes, yet their serial nature limits their use in imaging applications to samples comprised of only a few analytes.[11,12]

(1) Kane, R. S.; Takayama, S.; Ostuni, E.; Ingber, D. E.; Whitesides, G. M. *Biomaterials* **1999**, *20*, 2363−76.
(2) Khademhosseini, A.; Suh, K. Y.; Jon, S.; Eng, G.; Yeh, J.; Chen, G.-J.; Langer, R. *Anal. Chem.* **2004**, *76*, 3675−3681.
(3) Yeo, W.-S.; Yousaf, M. N.; Mrksich, M. *J. Am. Chem. Soc.* **2003**, *125*, 14994−14995.
(4) Zhang, S.; Yan, L.; Altman, M.; Lassle, M.; Nugent, H.; Frankel, F.; Lauffenburger, D. A.; Whitesides, G. M.; Rich, A. *Biomaterials* **1999**, *20*, 1213−1220.
(5) Whitesides, G. M.; Ostuni, E.; Takayama, S.; Jiang, X.; Ingber, D. E. *Annu. Rev. Biomed. Eng.* **2001**, *3*, 335−373.
(6) Ostuni, E.; Yan, L.; Whitesides, G. M. *Colloids Surf., B* **1999**, *15*, 3−30.
(7) Prime, K. L.; Whitesides, G. M. *Science* **1991**, *252*, 1164−7.
(8) Herrwerth, S.; Eck, W.; Reinhardt, S.; Grunze, M. *J. Am. Chem. Soc.* **2003**, *125*, 9359−9366.
(9) Lopez, G. P.; Biebuyck, H. A.; Harter, R.; Kumar, A.; Whitesides, G. M. *J. Am. Chem. Soc.* **1993**, *115*, 10774−81.
(10) Zhu, H.; Snyder, M. *Curr. Opin. Chem. Biol.* **2003**, *7*, 55−63.
(11) Elwing, H. *Biomaterials* **1998**, *19*, 397−406.

Imaging ellipsometry and surface plasmon resonance (SPR) are also commonly used to detect protein adsorption; however these methods, in addition to their intrinsically limited spatial resolution, also require a detailed knowledge of analyte optical properties (index of refraction) in order to make estimates of mass coverage, which are not always known and difficult to estimate for many proteins.[13,14] Secondary electron microscopy is a microcharacterization technique that is seemingly well suited to the task of quantifying protein adsorption on patterned organic thin-film arrays.[15] The escape depth of secondary electrons from a metal surface, for example, is relatively short (5−15 Å) and therefore in principle provides a sensitive measure through which to detect and quantify variations in the chemical nature of a metal surface.[16] It is known that adsorbed thin films can strongly modulate the SE yield of a metal surface,[17] and imaging of different SAMs on gold has been shown to produce large contrast differences depending upon the functionalization of the SAM used.[15] The relative nature of the image contrasts seen in SEM (absolute intensities are difficult to quantify) requires that the SAMs (as well as proteins) be patterned such that regions of the surface contain at least two areas with markedly differing chemical composition (and/or, mass coverage). This type of sample can be difficult to fabricate and only increases in complexity with the number of SAM compositions and bound proteins that are screened.

The surface sensitivity of SEM relies on a variety of factors which can affect the image contrasts seen for systems of the type shown schematically in Figure 1. These include the overlayer thickness, its average Z ratio (i.e., composition), electronic structure, and surface work function.[18,19] Disentangling these different contributions to the SEM image intensity is by no means trivial, but it does follow that the resulting SEM images embed potentially important information about the nature of an adsorbate film. It is a useful property of SAMs on Au, in this regard, that the samples are extremely smooth and thus minimize image contributions due to sample topography. This low background is an essential requirement for methods developed in this work that allow the quantification of SEM image contrasts in terms of adsorbate molecular properties.

Using a series of SAM and polymer overlayers, we demonstrate that varying quantitative contributions to the image contrast follow from the nature of the adsorbate mass coverage and composition, providing direct correlations with independently derived measurements of surface free energies (e.g., Kelvin probe and contact angle)[20] and adsorbate coverages measured by ellipsometry. These results support and extend suggestions made in earlier reports[9,15] and establish foundations for a novel image-based and potentially quantifiable approach

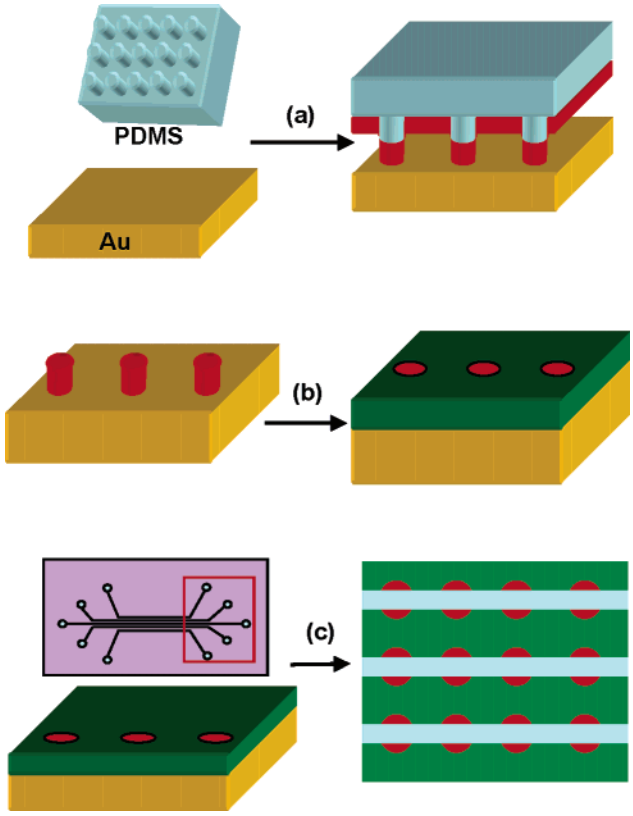

Figure 1. Steps for fabricating micropatterned protein arrays on microcontact printed thiol monolayers: (a) μCP alkane thiol on Au; (b) Backfill patterned region with complimentary monolayer; (c) Pattern protein using overlaid microfluidic channels.

to the detection of protein adsorption processes that require no spectroscopic (fluorescent) label. This method further circumvents the noted capabilities of metal and semiconductor surfaces to quench fluorescence,[21] a fact that has served to limit the utility of SAMs as an enabling chemistry for constructing biological assays based on this method of detection.[22]

We use multiple patterning steps based on soft-lithography to fabricate samples suitable for SEM analysis, specifically a combination of microcontact printing (μCP)[23] and micro-fluidic (μ-Fl) patterning[24] (Figure 1). The patterning of SAMs at the micron scale via microcontact printing is well established.[23] We make specific use of Au surfaces patterned with an array of hydrophobic alkanethiolate domains (which strongly promote nonspecific protein adsorption) within a more hydrophilic inert background and specifically functionalized regions that provide means to modulate patterns of protein adsorption.[6,22] The protein exposure in this work is spatially controlled using microfluidic channels (fabricated in polydimethyl-siloxane, PDMS) that are placed in contact with a patterned SAM array on Au (Figure 1c). This method allows the analysis of multiple protein affinities toward functionalized substrates with high spatial resolution. These model protein binding assays validate protocols for quantifying the image contrasts seen by SEM, a here-to-for unexplained property holding a more generalizable utility for screening complex combinatorial arrays.

(12) Lin, Y.; Wang, J.; Wan, L.-J.; Fang, X.-H. *Ultramicroscopy* **2005**, *105*, 129−136.
(13) Jung, L. S.; Campbell, C. T.; Chinowsky, T. M.; Mar, M. N.; Yee, S. S. *Langmuir* **1998**, *14*, 5636−5648.
(14) Tengvall, P.; Lundstrom, I.; Liedberg, B. *Biomaterials* **1998**, *19*, 407−422.
(15) Lopez, G. P.; Biebuyck, H. A.; Whitesides, G. M. *Langmuir* **1993**, *9*, 1513−16.
(16) Goldstein, J. I.; Newbury, D. E.; Echlin, P.; Joy, D. C.; Fiori, C.; Lifshin, E. *Scanning Electron Microscopy and X-ray Microanalysis*; Plenum Press: New York, 1981; p 673.
(17) Saito, N.; Wu, Y.; Hayashi, K.; Sugimura, H.; Takai, O. *J. Phys. Chem. B* **2003**, *107*, 664−667.
(18) Robinson, V. N. E. *J. Phys. D: Appl. Phys.* **1974**, *7*, 2169−73.
(19) Seiler, H. *J. Appl. Phys.* **1983**, *54*, R1−R18.
(20) Evans, S. D.; Urankar, E.; Ulman, A.; Ferris, N. *J. Am. Chem. Soc.* **1991**, *113*, 4121−31.
(21) Lakowicz, J. R. *Anal. Biochem.* **2005**, *337*, 171−194.
(22) Foley, J.; Schmid, H.; Stutz, R.; Delamarche, E. *Langmuir* **2005**, *21*, 11296−303.
(23) Xia, Y.; Whitesides, G. M. *Annu. Rev. Mater. Sci.* **1998**, *28*, 153−184.
(24) Kane, R. S.; Stroock, A. D.; Jeon, N. L.; Ingber, D. E.; Whitesides, G. M. *Soft Lithography and Microfluidics*; Elsevier: 2002; p 615.

Experimental Section

Reagents. Unless otherwise specified, reagents were used as received without further purification. Bovine serum albumen (BSA), γ-globulin (bovine), fibrinogen (bovine), and lysozyme (chicken) were purchased from Sigma. Phosphate buffered saline (PBS) and Dulbecco's phosphate buffered saline (DPBS) were purchased from HyClone. Poly-dimethyl siloxane (PDMS, Dow Corning Sylgard 184) was purchased from Ellsworth Adhesives. Octanethiol (C_8), decanethiol (C_{10}), and dodecanethiol (C_{12}) were purchased from Aldrich, while tetradecanethiol (C_{14}) and hexadecanethiol (C_{16}) were purchased from Fluka. Different thiol-terminated poly(ethyleneglycol)s (PEG_{2K}, Mw = 2 kDa, PEG_{5K}, Mw = 5 kDa, and an amine terminated PEG−mPEG, Mw = 2 kDa) were purchased from Nektar Therapeutics. Deionized (DI) water (18m Ω) was generated using a Millipore Milli-Q Academic A-10 system. Hexa-(ethyleneglycol)-undecanethiol (PEG_6) was synthesized using literature procedures.[25]

Substrate Preparation. Silicon wafers (100) were cut into pieces (~3 cm × 3 cm) and cleaned by immersion in a freshly prepared piranha solution (300 mL H_2SO_4: 100 mL HOOH. **Caution!** *Piranha solution is a strong oxidant and reacts violently with organic compounds; handle with care*). The substrates were rinsed with DI water and methanol and dried under a stream of nitrogen. A titanium adhesion layer (20 Å) was deposited onto the wafers using an electron beam source (Temscale FC-1800) followed by the evaporation of gold (2000 Å). The substrates were cleaned prior to use using a UV-ozone exposure (UVOCS T10 × 10) of 5 min.

Patterned SAMs. The general procedure for microcontact printing has been described previously.[23] The stamps were inked with an ethanolic solution of alkane thiol (10 mM) for 5 min and then placed into conformal contact with a freshly cleaned gold substrate for 30 s (Figure 1a). After removing the stamp, the substrate was rinsed with ethanol and dried under nitrogen. The patterned substrate was then immersed in an adsorbate solution (1 mM alkanethiol or 10 mg/mL polymer) for 30 min to backfill the unpatterned regions of the surface (Figure 1b).

When comparing the protein resistance afforded by different backfilling solutions, we found it useful to prepare several samples on a single substrate (this ensures identical brightness and contrast settings for the electron microscope). To do so, an array of samples was prepared on a common gold substrate, carrying out the second adsorption step using a macroscopic PDMS stencil mask. The latter mask was made by cutting holes in a PDMS slab (~2−3 mm in diameter). These holes were used as reservoirs for the different aqueous PEG (or polymer) solutions used to backfill the open region of the SAM pattern. After an allotted exposure time (30 min), the reservoirs were rinsed with buffer solution, the mask was removed, and the substrate was rinsed with buffer and finally dried under a stream of nitrogen.

Polymer Preparation. An *n*-hydroxysuccinimide (NHS) functionalized polyacrylamide (PAN, MW ~5 kDa) prepolymer was synthesized via the free radical polymerization of acrylamide and acryloxyhydroxysuccinimide following literature procedures.[26] This polymer (100 mg) was then reacted in a buffered (pH ~7) aqueous solution (2 mL) containing varying relative ratios of 3-methyl(thiopropylamine) (MTP) and a methyl-terminated poly(ethylene glycol) amine (mPEG) with a molecular weight of ~2 kDa (2× excess total amine concentration relative to the NHS ester). The reported relative percent mPEG values reflect the amine ratios reacted with the active ester functionalized prepolymer. Excess ligand was removed by precipitating the polymer with cold tetrahydrofuran, decanting off the supernatant solution, and resuspending the polymer in buffer several times. Detailed characterizations of these modified acrylamide polymers will be reported separately.

Ellipsometric Measurements. Gold slides were placed into buffered adsorbate solutions (either polymer or protein) for 30 min, after which they were thoroughly rinsed with Millipore water and dried under a stream of nitrogen. Thicknesses were measured using a Gaertner L116C ellipsometer utilizing a HeNe laser with a wavelength of 6328 Å and an assumed thin film refractive index of 1.45. Reported thicknesses are an average of several measurements made over different regions of a sample.

Protein Adsorption. A series of microfluidic channels (15 μm tall × 90 μm wide) were made in a slab of PDMS using literature procedures.[27] These channels were placed into contact with a freshly patterned substrate (Figure 1c) and then filled by placing a protein solution (0.1 mg/mL) in the filling reservoir at the end of the channel and blocking the other end of the channels with a slab of PDMS. The capillary outgas technique (COT) was used to draw the solutions in the filling reservoirs through the channels.[28] The protein solutions were left in contact with the surface for 30 min after which the channels were drained and refilled 3 times with buffer solution. Following these rinsing steps, the channel network was peeled away from the substrate, and the entire sample was rinsed with Millipore water and then dried under nitrogen.

SEM Imaging. Substrates were imaged using a JEOL-6060LV scanning electron microscope using a primary electron beam energy of 5 kV. Grayscale images were recorded with 8 bit resolution at a magnification of 650×, with a total acquisition time of 2 min. Grayscale calibration references were created on the sample by exposing a small portion of the image field (typically a zone 5 μm × 8 μm in size) to the electron beam for 3 min (magnification of 20 000×). The image contrast and brightness settings were adjusted using that reference to provide an image that had maximal contrast without under- (or over-) saturating the detector response.

Image Analysis. The acquired images were analyzed using Adobe Photoshop 7.0 and ImageJ 1.33u to measure the relative grayscale intensities of regions of interest. The dark grayscale reference region and the patterned HDT regions were used as calibration points to set the 0% and 100% linear detector response levels in the image, respectively. The image analysis data are reported as a percentage relative to the intensity scale defined by the calibration intensities of these two regions.

Results

Past work has shown that SAMs can produce significant composition-dependent variations in the contrast seen in SEM images of surfaces.[15] This sensitivity is easily seen in a composite overlay (Supporting Information Figure S1) of the secondary electron yields collected with similar operating parameters of the microscope for three Au surfaces bearing different SAM overlayers (Au, C_{16}, and PEG_6). An interesting trend in these data is that the brightest image intensity comes from the C_{16} SAM and that, despite their similar mass coverages (as determined ellipsometrically), the composition differences of the C_{16} and PEG_6 SAMs yield markedly different grayscale intensities. These latter trends can be explained more systematically by examining the image intensities of a series of alkanethiol SAMs.

Figure 2 shows a series of representative SEM images of alkanethiolate SAMs on gold patterned by μCP along with line scan analyses of their respective grayscale image intensities. In these samples, 30 μm diameter circles of hexadecane thiol (C_{16}) were patterned by μCP followed by backfilling the sample with a variety of different chain length alkane thiols (C_8 and C_{16}).

(25) Pale-Grosdemange, C.; Simon, E. S.; Prime, K. L.; Whitesides, G. M. *J. Am. Chem. Soc.* **1991**, *113*, 12−20.
(26) Pollak, A.; Blumenfeld, H.; Wax, M.; Baughn, R. L.; Whitesides, G. M. *J. Am. Chem. Soc.* **1980**, *102*, 6324−36.
(27) Fosser, K. A.; Nuzzo, R. G. *Analytical Chemistry* **2003**, *75*, 5775−5782.
(28) Monahan, J.; Gewirth, A. A.; Nuzzo, R. G. *Anal. Chem.* **2001**, *73*, 3193−7.

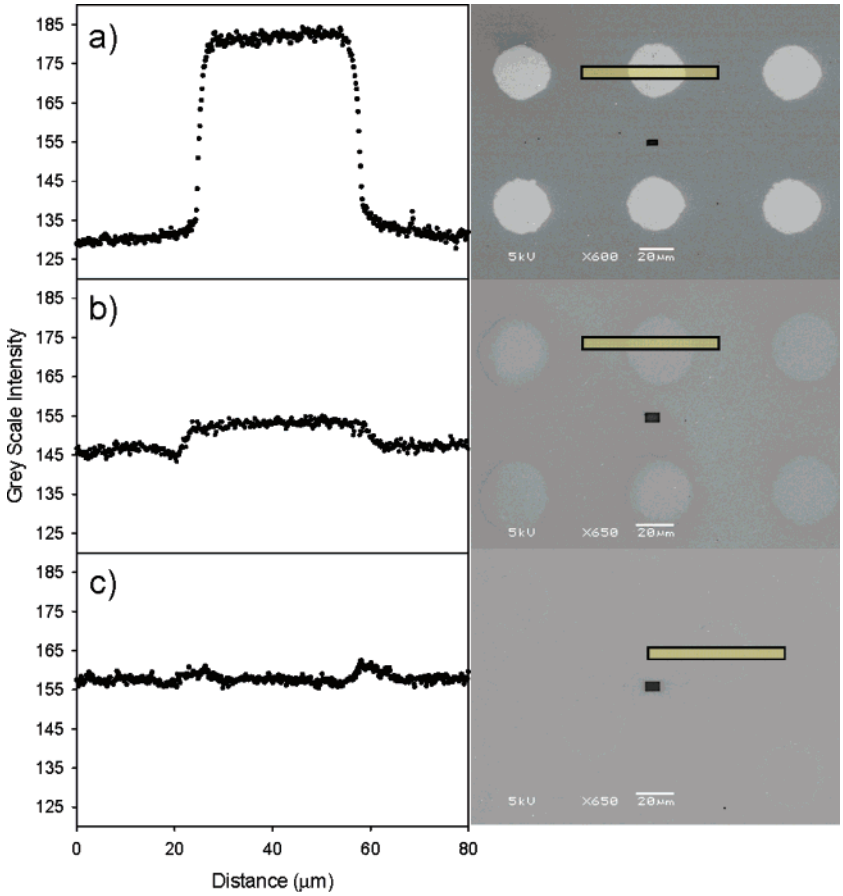

Figure 2. SEM micrographs of μCP alkane thiols on gold along with their respective image intensity line scans: (a) Hexadecane thiol on clean Au (Au/C_{16}); (b) Hexadecane thiol with octane thiol backfill (C_8/C_{16}); (c) Hexadecane thiol with hexadecane thiol (C_{16}/C_{16}) backfill.

The contrast differences between the printed C_{16} region and the surrounding unpatterned areas are both marked and strongly chain-length dependent. The high contrast seen in the blank Au−C_{16} pairing is progressively softened as the samples are backfilled with C_8 and C_{16} thiols. It is interesting to note that the sample backfilled with a C_{16} solution (Figure 2c) shows essentially no contrast difference with the exception of a slightly brighter annulus present at the edges of the printed features.

These intensity profiles can be directly correlated to several surface properties of SAMs, each of which speaks to the nature of specific factors involved in the contrast mechanisms. The normalized grayscale intensities for a larger series of *n*-alkane thiol SAMs on Au are plotted against advancing contact angles of hexadecane (Figure 3a)[29] and literature values of surface potential determined by Kelvin probe (Figure 3b).[30] Each measure provides insights as to the surface free energies of the various SAMs. As the data in the figures illustrate, there exists a very sensitive and direct correlation between the secondary electron yields (as defined by the SEM image intensities) and other fundamental surface properties of the samples (e.g., wetting).

In this case, the chain-length dependence evidenced is one related to chain structure, namely the well understood dependence of chain order on the length of the alkyl chain,[31] the order in this case being highest for the C_{16} SAM. The fact that the C_{16} layer is brighter than the subsequently shorter layers in this example is an important observation which hints at a more complex mechanism of SEM image contrast other than simple electron attenuation by an organic overlayer.

To further examine the effects of organic thin films on SEM contrast, a second system affording very different film chemistry from the well ordered alkanethiol SAMs was observed. A series of functionalized acrylamide polymers was synthesized with varying amounts of MTP and mPEG grafted to the polymer backbone, the structure of which is depicted schematically in Scheme 1.

The PAN precursors used to synthesize the adsorbates had ∼5 NHS active ester groups per ∼70 acrylamide segments. The grafting reaction produces side chain functionalities distributed statistically at levels somewhat less than this (the couplings are not 100% efficient due to competing hydrolysis). These polymers were used to backfill the patterned C_{16} samples and imaged in the SEM. The resulting intensity analysis data along with the ellipsometrically determined thicknesses of the polymer films are shown in Figure 4. The image intensity decreases by almost 30% as the relative amount of the grafted mPEG on the polymer decreases; the polymer overlayer increases in thickness in this same order. These trends are qualitatively opposite from those seen in the alkanethiol SAM samples which suggests the mechanism responsible for image intensity is different for the two systems of adsorbates. The polymer overlayers are all extremely (and essentially indistinguishably) hydrophilic and,

(29) Laibinis, P. E.; Whitesides, G. M.; Allara, D. L.; Tao, Y. T.; Parikh, A. N.; Nuzzo, R. G. *Journal of the American Chemical Society* **1991**, *113*, 7152−67.
(30) Evans, S. D.; Ulman, A. *Chem. Phys. Lett.* **1990**, *170*, 462−6.
(31) Dubois, L. H.; Nuzzo, R. G. *Annu. Rev. Phys. Chem.* **1992**, *43*, 437−63.

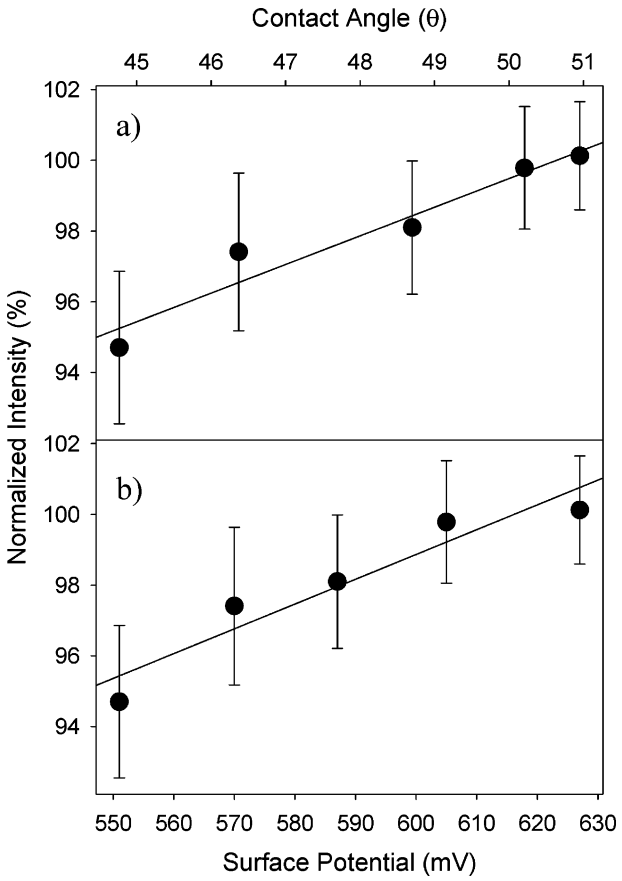

Figure 3. Normalized SEM intensity of *n*-alkane thiol monolayers linearly correlated with (a) hexadecane contact angle and (b) surface potential.

Scheme 1. General Reaction for Grafting Primary Amines (MTP and mPEG) to NHS Modified Polyacrylamide Prepolymers

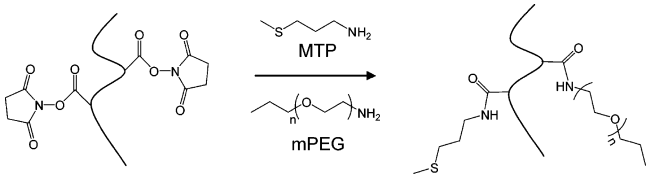

to a first approximation, present an essentially uniform profile of thin-film compositions at the interface. The electron scattering cross-sections, with one possible exception, are not expected to be severely impacted by the composition changes imparted to the overlayer by the varying PEG content, and thus the observed intensity is believed to be dictated by film thickness alone. One important caveat that has to be considered in the context of this model is that the sulfur atom of the MTP thioether segment (and its bonding at the Au surface) strongly dictates the surface potential at the metal interface (as observed in Figure 2a for alkanethiols) and must be accounted for when comparing SE intensities, as this bonding is a major contributing factor in determining SE yield with minor corrections from other parameters such as film thickness and composition.

In addition to studying fundamental sources of SEM image contrast, these patterned substrates provide an ideal model system for investigating the utility of SEM as a means for quantifying protein interactions with functionalized surfaces. Figure 5a shows a representative SEM image of a patterned Au surface after being exposed (using a series of microfluidic channels) to four different protein solutions. The bright areas

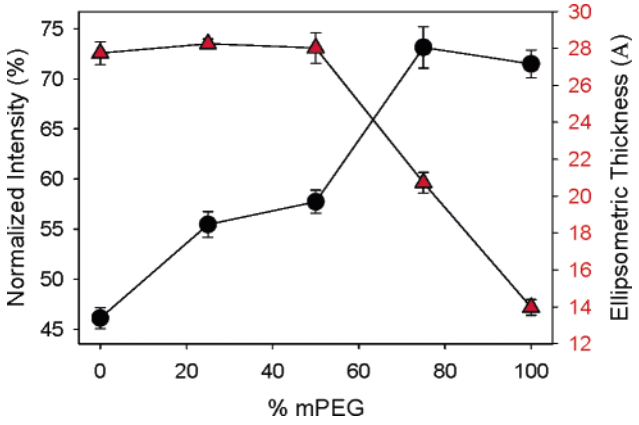

Figure 4. Normalized SEM image intensities of mPEG/MTP modified polyacrylamide polymers (left). Values are normalized between hexadecane thiol (100%) and the primary beam contaminated reference area (0%). Ellipsometric thickness of mPEG/MTP grafted polymers (right).

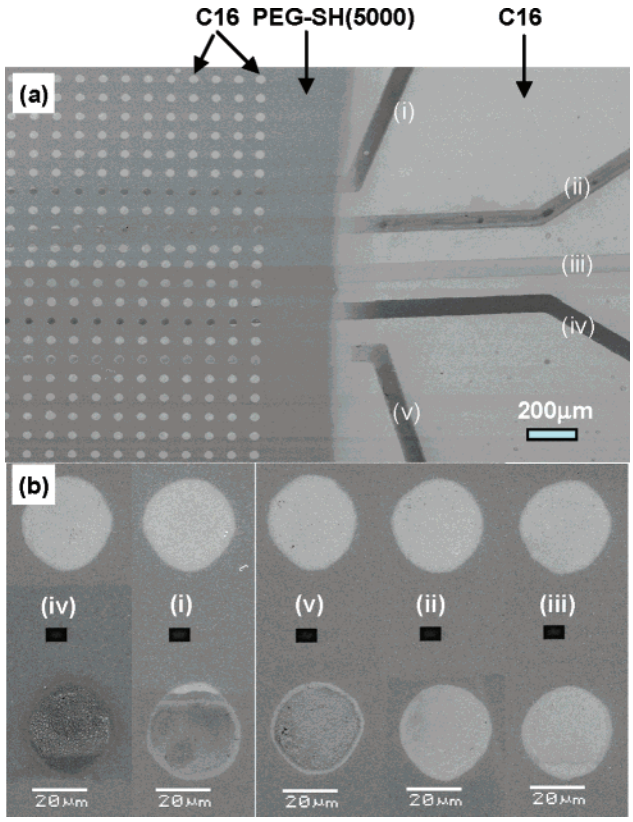

Figure 5. SEM micrographs of protein adsorbed onto μCP alkane thiol arrays: (a) Low magnification view of C_{16} arrays with a PEG_{5k} monolayer backfill; (b) High magnification composite image of channel regions showing protein adsorbed onto hexadecane thiol: (i) BSA; (ii) lysozyme; (iii) DPBS; (iv) fibrinogen; (v) γ-globulin.

of the image denote regions bearing a C_{16} SAM. The large bright area of this image corresponds to C_{16}−SH ink that was transferred to the surface from an unpatterned region of the printing stamp. The large dark region in this case is comprised of a PEG_{5k} SAM which serves as a background domain that resists protein adsorption. This sample then provides a simple model of a protein assay that can be used to follow patterns of nonspecific adsorption. Protein adsorption is clearly visible in regions where the liquid streams in the microfluidic channels overlaid on the sample. The contrast changes are most pronounced in the C_{16} SAM regions indicating significant protein

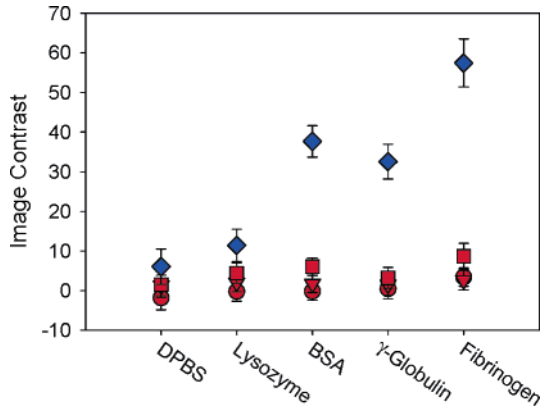

Figure 6. Normalized SEM image intensity analysis of proteins adsorbed onto different patterned SAM Au surfaces: C_{16} regions exposed to protein solutions (blue: (◆) HDT); PEG SAMs exposed to protein solutions (red: (■) PEG_{5k}; (▼) PEG_{2k}; (●) PEG_6).

adsorption in these regions. A higher magnification set of images taken from the patterned regions is shown in Figure 5b.

These representative images allow a direct side-by-side comparison of the areas (C_{16} SAM and PEG_{5k} resist) that were exposed to the various protein solutions and an adjacent reference zone protected from the solutions by the PDMS structures of the microfluidic channels. The upper half of this composite image corresponds to C_{16} and PEG_{5k} regions that were held in contact with the PDMS of the microfluidic stamp; the lower half are those that had been protein exposed. In these data, even though identical concentrations of proteins were used (0.1 mg/mL), the domains are marked by a significant variation in image contrast. Little grayscale variation is seen in the regions bearing the PEG_{5k} film, a result suggesting that this latter SAM provides a significant inhibition of nonspecific adsorption.

Intensity analyses of the C_{16} printed regions from data similar to that shown in Figure 5b, but using three different PEG inert backgrounds (PEG_6, PEG_{2K}, and PEG_{5K}), are plotted in Figure 6. These data are plotted as image contrast, here defined as the difference in average normalized SEM intensity between a region that was not protein exposed (i.e., upper half of Figure 5b) and a region that interacted with a protein solution (i.e., lower half of Figure 5b). The reported contrast for the C_{16} SAM regions (blue) is the average of the C_{16} regions in the three different samples, each fabricated using a different inert background layer. These data clearly suggest that the SEM response is not unique for all proteins. The trends, in fact, directly correlate with protein uptake deduced via independently measured ellipsometric data (Supporting Information Table S1). A similar analysis made of the inert background regions (red) shows little contrast change is evidenced for all of the proteins studied here (values corresponding to less than ~5% seen for adsorption on a C_{16} SAM surface). These results support and extend understandings described in the literature for PEG-based SAMs[7] and establish that grayscale intensities measured by SEM, when properly referenced, can be used to follow subtle changes in coverage qualitatively and perhaps semiquantitatively as well.

As a control experiment, an identical set of samples bearing patterned C_{16} SAMs, but omitting any sort of backfilling inert (PEG) monolayer, was prepared. The SEM images of these samples indicate protein adsorption occurs in a significant way in both the regions covered with a C_{16} SAM as well as in the

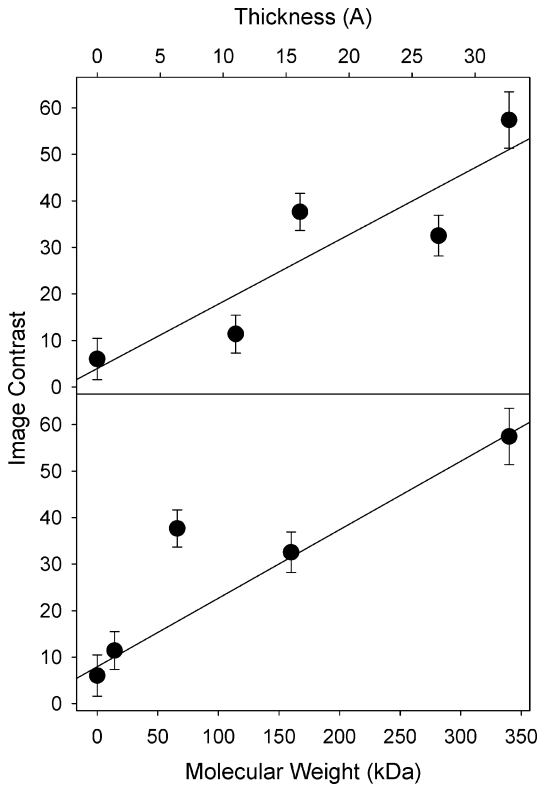

Figure 7. Molecular weight dependence of normalized SEM image contrasts of proteins adsorbed on C_{16} arrays on Au: (a) Image intensity correlated to protein mass coverage; (b) Image intensity correlated to protein molecular weight.

regions with no film present (Supporting Information Figure S2). The intensity of the microfluidic channel regions show significant SE attenuation for all of the proteins investigated, while the buffer filled channel shows almost no contrast change relative to the background. These results are consistent with the data of Figure 5 and confirm an attenuation mechanism in which the higher organic overlayer coverage that results from protein adsorption leads to a decrease in the SE yield for both bare gold and SAM patterned surfaces.

The protein specific responses can be correlated with both molecular weight and film thickness (measured ellipsometrically), as shown in Figure 7. The observed intensity changes generally trend with mass coverage changes (Figure 7a), which in each case follow changes in molecular size (Figure 7b). This again provides strong support for a mechanism dominated by the attenuation of the SE yield (which largely originates from the underlying Au) due to the presence of organic overlayers of different thicknesses, a model somewhat different and inversely varying with the chain-length dependent data obtained for pristine alkanethiolate SAMs (Figure 3). From these results, it is evident that SEM is sensitive to protein mass coverage changes, which offers the possibility of using SEM visualization as a quantitative protein assay tool. This utility was tested in two model studies.

We first examined the concentration dependence of the adsorption of fibrinogen onto a C_{16} SAM (Figure 8). These data show that increasing the protein concentration is marked by increases in SE contrast relative to that of an unexposed C_{16} monolayer (Figure 8a). Intensity analyses for these data are plotted in Figure 8b, where the contrasts (intensity difference

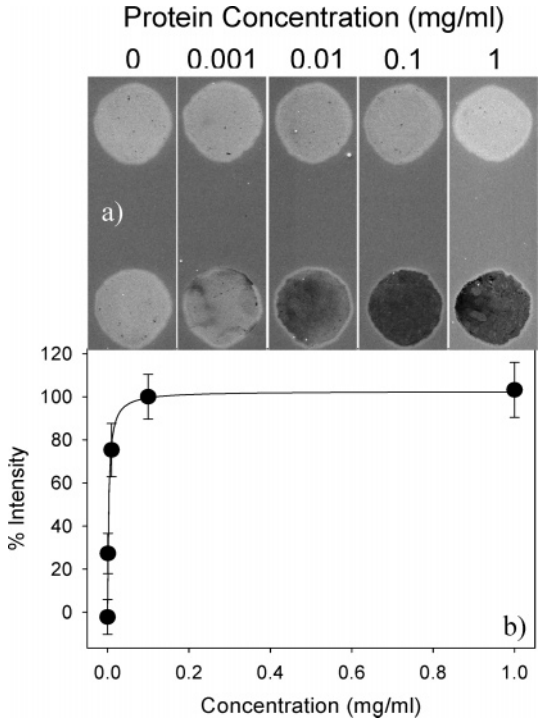

Figure 8. Concentration dependent fibrinogen adsorption onto C_{16} monolayers: (a) Composite SEM image of C_{16} arrays exposed to fibrinogen; (b) Normalized image intensity of fibrinogen submonolayers.

between a pristine C_{16} region and a protein exposed C_{16} region) have been normalized by the maximum contrast observed at 0.1 mg/mL. Fitting this response to a classical Langmuir isotherm yields an apparent dissociation constant (K_D) of 9.3 $\times$ 10^{-9} M (that is to say that the binding is essentially irreversible).

The second study involves the specific adsorption of avidin onto a monolayer consisting of biotin-functionalized BSA (b-BSA). These data consist of a composite image of microfluidically patterned lines of both biotinylated and nonbiotinylated BSA residing on top of an HDT monolayer. Half of this pattern was then immersed in an avidin solution, and SEM images were collected to quantify both the specific interaction between the biotin−avidin conjugate and, as a reference, the nonspecific adsorption of the avidin on the HDT background. As can be seen in the composite image, the proteins are essentially uniform in contrast prior to avidin exposure, yet after exposure, the biotin-labeled protein monolayer darkens considerably relative to the nonfunctionalized BSA channel (Figure 9). These data were taken on the same Au substrate under identical microscope conditions such that direct relative intensity comparisons can be made. Referencing the images to the dark reference and HDT monolayer background, however, allows a full quantitative analysis of film coverages. Using the thickness correlations elucidated from Figure 7a, the avidin-induced increase in thickness on the b-BSA was found to be ~25 Å, which agrees well with literature values for avidin binding in this type of affinity assay.[32] By comparison, <10 Å of the avidin was found to bind nonspecifically to the unlabeled BSA channel. This simple model assay therefore demonstrates the feasibility of SEM as a quantitative tool for studying high specificity, protein affinity interactions.

(32) Ebersole, R. C.; Miller, J. A.; Moran, J. R.; Ward, M. D. *Journal of the American Chemical Society* **1990**, *112*, 3239−41.

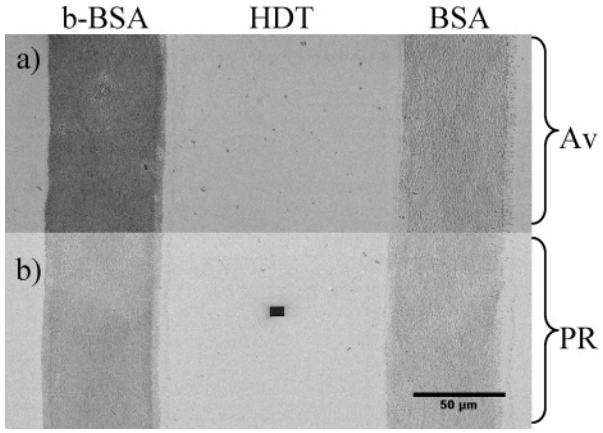

Figure 9. Composite SEM image of specific avidin adsorption onto μ-Fl patterned biotinylated-BSA (b-BSA, left) and BSA (BSA, right) films nonspecifically bound to an HDT SAM background: (a) avidin exposed region (Av); (b) pristine region (PR).

These studies offer valuable insights into the mechanisms that determine the SEM image contrasts seen for patterned organic thin film arrays (including those derived from proteins) on Au, understandings that are generalizable to other surfaces as well. These findings further provide a means through which image contrast for samples involving surface-adsorbed proteins can serve as arguments for changes in surface composition and coverage as are frequently required in bioanalytical assays.[33]

Discussion

This work examines in a quantitative fashion the utility of using SE yields as a means for quantifying thin organic film coverages on Au, especially for systems holding promise for use in protein bioassays.[34] The model systems adopted in this work, while simpler than would be the case for a true surface binding assay, do serve to illustrate the factors that are most important for such a system.

SEM Image Contrast. In an SEM experiment, bombardment by primary electrons with an energy of several keV ($E_{primary}$) results in the emission of electrons from the target material over a range of energies from zero up to $E_{primary}$.[16] The electron flux emerging from the sample contains many contributions, including elastically and quasi-elastically scattered electrons, as well as Auger electrons, among others.[19] It is typical that secondary electrons are defined as those emitted with energies below ~50 eV.[16] The higher energy electrons, consisting primarily of inelastically backscattered and elastically reflected electrons, contribute prominently to excitations leading to secondary electron emission and significantly contribute to the total SE emission signal. This is the basis of the mechanism of bulk materials contrast commonly observed in SEM images, as the backscattering coefficient (η) often varies more as a function of material than does the secondary emission yield (δ) resulting from primary beam excitation.[18,19] This complex factor must be taken into account when one tries to analyze SEM image intensities due to the fact that small changes in η can have dramatic effects on the total SE yield. In the present case, however, given that the total interaction volume (depth) of the

(33) Senaratne, W.; Sengupta, P.; Harnett, C.; Craighead, H.; Baird, B.; Ober, C. K. *NanoBiotechnology* **2005**, *1*, 23−34.
(34) Varnum, S. M.; Woodbury, R. L.; Zangar, R. C. *A protein microarray ELISA for screening biological fluids*; Humanna Press: New Jersey, 2004; Vol. 264, p 161−172.

backscattered electrons is large compared to the organic film thicknesses being analyzed, such impacts are not expected to be a major contributing factor to the total SE yield. The variations in the SE yield found here, then, must relate to factors depending more on the nature of the target material in regions lying near the surface.

As can be seen from the data in Figure 2, the secondary electron yield from a metal (Au) is exquisitely sensitive to chemical modifications made at its surface. Such effects have been discussed in considerable detail in the literature, and in general terms, the underlying mechanisms have been assumed to be sufficiently complex so as to preclude meaningful materials analysis based on the measurement of SE yields alone.[9,15] The well-defined surfaces afforded by SAMs, however, provide a degree of control that could alter this proscriptive outcome. One might expect, for example, given the 5−50 eV energies of the secondary electrons and in analogy to photoelectron spectroscopy, that an overlayer deposited on top of a metal surface would attenuate the electron yield due to the short mean free paths of electrons in this energy range. We see in the present data trends that stand in marked contrast to this expectation. When an alkanethiolate SAM is formed on a gold surface, the secondary electron yield is significantly increased relative to that of an unmodified gold surface (Figure 2a), an enhancement that actually increases with the chain length of the SAM (longer chains appear brighter). While not negating the importance of attenuation effects, there clearly exist circumstances where SE yields can be increased by a thin attenuating overlayer.

Prior studies have shown that alkane thiol modified metal surfaces have dramatically altered surface potentials, ones that depend strongly on the structure of the SAM.[30,35] The contrasts seen in Figure 2 can be explained in this way and reflect the fundamental ways in which the thiol bonds to the Au metal surface. The work function in the region of the printed alkanethiolate SAM is lowered relative to the surrounding unmodified regions, thereby leading to a higher electron count being seen there, even though this region bears a thicker overlayer. The literature suggests two factors that might be affected by the SAMs chain-length dependent modification of the Au work function. First, the kinetic energy distribution of the SEs (dN/dE) will be altered according to a functional form approximated by eq 1

$$\frac{dN}{dE} = k\cdot\frac{(E - E_F - \Phi)}{(E - E_F)^4} \qquad (1)$$

where the energy distribution is related to specific properties of Au via the material constant k, the primary electron energy E, the Fermi energy E_F, and the work function Φ.[36] The formation of a SAM would have its largest impact here by narrowing the kinetic energy distribution of the SEs slightly. The chain length dependence of Φ is a much more modest effect, varying by approximately 0.20 eV between a C_8 and a C_{16} alkanethiolate SAM.[30,35] However, the impact of this difference would be large on the effective cross section for SE emission in a fashion analogous to thermionic emission. In this context, the yield would follow the form of eq 2

$$i_{SE} \propto A\cdot T^2\cdot e^{-\Phi/kT} \qquad (2)$$

where the SE current (i_{SE}) scales according to an exponential dependence on Φ (or difference there in) and the effective hot electron energy (kT), with A being a materials constant and temperature (T).[37] The differences evidenced for a chain-length dependent series of SAMs (Figure 3b) fall well within the linear region of this exponential dependence (being of the order of 5% of the full range grayscale intensity for the ∼200 meV difference in surface potential measured across this series of SAMs). With these relationships in mind, it is apparent that the gross work function change of the surface is determined by the formation of the S−Au bond, as evidenced by the very large contrasts seen between an Au and C_{16} surface (Figure 2a). Mixed thiol surfaces (C_8/C_{16}) reveal much smaller contrasts, which reflect slight corrections to the work function based upon the chain length of the particular SAM being imaged (Figure 2b). The pattern of contrasts seen for these data is therefore well described by this model of the SE yield.

One aspect of the data shown in Figure 2 remains poorly understood, namely that while the C16/C16 sample (Figure 2c) shows no contrast difference, it exhibits a set of faint rings of brighter intensity around the microcontact printed regions. We believe this relates to the presence of subtle monolayer structural variations caused during the printing process, which contribute to the grayscale contrast of the SEM on the basis of the slight work function differences they induce. It is most intriguing that the annulus seen there is bright relative to other regions. The nature of the structural differences present in these regions remains incompletely understood.

A cautionary note also must be given regarding the data given for the mixed thiol samples in Figure 2, namely that there is most likely some degree of place exchange of thiols in the different regions of the patterned SAM. The microcontact printing process yields a structurally and compositionally well-defined SAM on the gold.[23] When these samples are placed in a solution of thiol, however, the printed SAM is modified due to exchange with thiols from the solution.[38] This will have the effect of reducing the grayscale contrasts observed in the SEM images, as the printed regions intermix with the complimentary thiol. For a long time exposure to the second thiol solution, the printed pattern will be lost, with little contrast observed. For this reason, the immersion time of a printed sample in the second thiol solution was kept to a minimum (∼30 min).

The simple work function model is an incomplete one given the fact that, at some limiting thickness value, the organic layer will begin to attenuate the SE yield of electrons originating in the Au substrate. These impacts are important and arise in a more complex way, one that convolves the influence of finite SE mean free paths in the organic overlayer together with features related to both the elemental composition of the film and its surface free energy (work function). The mechanisms through which an organic overlayer on Au mediates the SE yield (and thus grayscale image intensities) must have more determinates, given that not all adsorbate materials exhibit image intensities that directly correlate with thickness. We saw, for

(35) Alloway, D. M.; Hofmann, M.; Smith, D. L.; Gruhn, N. E.; Graham, A. L.; Colorado, R., Jr.; Wysocki, V. H.; Lee, T. R.; Lee, P. A.; Armstrong, N. R. *J. Phys. Chem. B* **2003**, *107*, 11690−11699.
(36) Chung, M. S.; Everhart, T. E. *J. Appl. Phys.* **1974**, *45*, 707−9.
(37) Briggs, D.; Seah, M. P. *Practical Surface Analysis Volume 1—Auger and X-ray Photoelectron Spectroscopy*, 2nd ed.; John Wiley & Sons: New York, 1983; Vol. 1, p 657.
(38) Chidsey, C. E. D.; Bertozzi, C. R.; Putvinski, T. M.; Mujsce, A. M. *J. Am. Chem. Soc.* **1990**, *112*, 4301−6.

example, in a system comprised of a series of polymer samples (Figure 4), that intensity (electron) attenuation follows variations in film thickness (albeit not quantitatively). The polymers in this case provide overlayers that are both comparable in composition and uniformly hydrophilic. With the MTP, as a thioether ligand, serving as an effective means for attaching these polymers to the Au surface, the various forms of grafting largely serve to bias the mass coverage.[39] The trend is such that thicker films appear darker, however, the correspondence is not precise given that the ellipsometric data for the polymer films exhibits two regimes (at high mPEG density, the thickness of the adsorbed films falls dramatically, from 28 Å to 14 Å). The systematic change in the MTP graft density in these polymers results in differences in the number of S−Au interactions present as the metal surface, which could lead to work function changes in the surface (analogous to the results for the alkane thiol case). Given this, one notes an almost 30% increase in intensity even as the relative number of S−Au interactions goes to zero. This large change in intensity cannot be explained by surface potential arguments alone and is qualitatively opposite from results seen in the alkane thiol data. In the limiting case of comparing the SE intensity of bare Au (no S−Au interaction) to a fully thiolated C_{16} SAM, the intensity increases, while, in the polymer case, the intensity decreases with increasing S−Au interactions (100% mPEG to 100% MTP). The polymer−Au interactions then must be dominated by those occurring with chain segments rather than the S atoms of the MTP grafts. From these data, it is apparent that the effects of effective surface potential and film thickness are intertwined such that the resulting image intensities are the consequence of a combination of these two factors with a very different weighting than was seen for the *n*-alkanethiolate SAMs.

These experiments establish two limiting behaviors: (a) SE yields dominated by chain-length dependences of surface potential in a series of structurally self-consistent *n*-alkane thiol SAMs on Au; and (b) the attenuation of the SE flux from the Au by a nominally uniform organic overlayer. The former can be understood in terms of a thermionic emission model, with surface potential being the primary determinant. The latter behavior is perhaps most familiar as that seen in an X-ray photoelectron spectroscopy experiment.

The simplest model of the Au−organic film system is to treat the interface as two discrete layers. Upon excitation of the SE from the Fermi level of the Au metal to the vacuum level, the SE is promoted to an environment that is essentially organic in nature. The probability of the SE interacting with and scattering within the organic thin film, prior to being emitted from the surface, is determined by fundamental properties of the film, such as its composition, density, and thickness. These properties can be expressed in terms of an electron attenuation length (λ) according to eq 3

$$\frac{I}{I_0} \propto e^{-d/\lambda} \tag{3}$$

where I and I_0 are the observed SE intensity and the unattenuated SE intensity of a pristine surface, respectively, and d is the overlayer thickness. The attenuation length embeds all the composition and electronic structure sensitive aspects of this mechanism of SE attenuation. To a first approximation, we can define this term according to eq 4

$$\lambda \propto \frac{E}{\frac{E_p{}^2}{E_p{}^2 + E_g{}^2}[Ln(\rho^{1/2}E)]} \tag{4}$$

where E_p is the plasmon energy, E_g is the band gap energy, E is the electron energy, and ρ is the density of the material.[40] Here, the influences of composition are also manifested in the plasmon energy (E_p) according to eq 5

$$E_p = \left(\frac{N_V \cdot \rho}{A}\right) \tag{5}$$

where N is the number of valence electrons in the material and A is the effective atomic number of a scattering overlayer.[40] In simple terms, the composition and density of the overlayer scale the number of electrons that serve to scatter the emerging SE flux. In general, across a broad range of organic compositions, the attenuation length for electrons with energies in the range of the SE's is of the order of 20 Å.[41] So then, because an overlayer comprised of a protein of even modest molecular weight, one expects very little difference in effective composition or density of the attenuating thin film, and if properly calibrated as to the instrument response, the grayscale contrasts for such systems are expected to vary simply as an exponential function of the mass coverage (thickness). For SE energies ranging from 5 to 50 eV, the mean free paths for attenuation in a molecular thin film are relatively modest but generally larger than the range of the dimensions of most proteins.[42] One expects then to see behaviors in the images that might vary from being linearly to more strongly correlated with an independent measure of mass coverage. The data presented in Figure 6 show largely linear correlations of the grayscale intensity changes seen when proteins were adsorbed onto a domain of C_{16} SAM on Au, following directly the thickness changes measured ellipsometrically (ranging from 11 Å to 33 Å nm, Figure 7a). Such thicknesses are well within the range where the predicted exponential form of the attenuation is expected to be reasonably well modeled by a linear approximation.

Protein Adsorption in SEM Images. The monolayer results indicate that the SE yield is dominated by an emission profile from Au that is mediated by soft segmental and other adsorbate-based interactions. Factors such as the effective composition of the overlayer and the nature of strong adsorbate-based bonding (for example, the high S-coverage afforded by the SAM) are all relevant. In the model adopted here, these factors are constructed to be self-referencing. The binding of a protein, for example, leaves the composition and bonding of the C_{16} SAM residing under it essentially unchanged. The fact that it layers the substrate with a more polar phase is an impact that arises self-consistently for each of the model proteins examined. The image contrasts then scale most prominently with changes in total overlayer thickness, which in turn provides a secondary

(39) Troughton, E. B.; Bain, C. D.; Whitesides, G. M.; Nuzzo, R. G.; Allara, D. L.; Porter, M. D. *Langmuir* **1988**, *4*, 365−85.
(40) Tanuma, S.; Powell, C. J.; Penn, D. R. *Surf. Interface Anal.* **2003**, *35*, 268−275.
(41) Lamont, C. L. A.; Wilkes, J. *Langmuir* **1999**, *15*, 2037−2042.
(42) Tanuma, S.; Powell, C. J.; Penn, D. R. *Surf. Interface Anal.* **1994**, *21*, 165−76.

correlation with the nature of the macromolecular adsorbates binding to the surface.

The sensitivity of the SEM images to the adsorption of macromolecules provides a relatively simple (and quantifiable) detection scheme for imaging studies of biological binding and recognition. More importantly, it is one that operates without requirements for the labeling procedures needed in more common fluorescence experiments. A simple demonstration of this capacity is illustrated by the nonspecific binding studies carried out using an SAM-based array. In this set of experiments, three different PEG surfaces were examined as protein resists, and when patterned in conjunction with the methyl terminated C_{16} SAM, the PEG surfaces offer maximal contrast in the SEM images by acting as an inert background upon protein exposure.

What is most remarkable about these latter data is the fact that the image contrast on the HDT regions strongly correlates with the molecular weight of the adsorbing protein; larger proteins adsorbing on the C_{16} SAM produce darker regions in the images (Figure 6). The four model proteins studied in these experiments have molecular weights that vary by over an order of magnitude (Supporting Information Table S1). For the case of fibrinogen, a relatively thick protein film is formed (~33 Å), which significantly attenuates the secondary electron emission from the gold surface relative to the pristine C_{16} monolayer (Figure 6). When a thinner film is formed, as seen with lysozyme (~11 Å), the secondary electron emission is attenuated less and appears brighter than a fibrinogen covered SAM in the images (Figure 5b). On this basis, the analytical figure of merit established by Figure 6 suggests contrasts could effectively speciate an unknown protein mass to within a range of ~25 kDa. There are caveats here, however, as illustrated by the contrast variations seen between the BSA and the γ-globulin films. Even though γ-globulin has a molecular weight nearly twice that of BSA and forms films that are significantly thicker than BSA, the two are virtually indistinguishable with regard to SEM contrast (Figure 5b). This discrepancy is most pronounced when intensity is plotted against molecular weight (Figure 7b), where the BSA value was treated as a statistical outlier relative to the linear fit of the other four data points. There are several possible reasons for this disagreement one being the dramatic isoelectric point difference between these two proteins. The adsorption experiments were performed in buffered solutions at pH 7.4, which leaves the γ-globulin (pI ~6.5) largely in a neutral state, while the BSA (pI ~4.7) has a significant negative charge. This residual charge can lead to a significant dipole being formed at the surface which we suspect alters the overall electron yield. The present experiments are not sufficient to establish the relative importance of this or other structure related effects.

Protein Assays via SEM. Quantitative protein assays require information as to the absolute amount of protein that is bound. Concentration-dependent protein studies were performed to explore the relative utility of SEM as an analytical tool for such assays. Fibrinogen was chosen as one model protein for this purpose because of its large film thicknesses, which offers a high dynamic range for the image contrast relative to the other proteins used in this study. As illustrated by the data given in Figure 8, increasing protein concentrations lead to increasing SEM image contrasts under identical exposure conditions. For the very dilute protein solutions, submonolayer coverages are observed as areas of uneven contrast within the C_{16} regions. This suggests that proteins initially bind in the form of complex heterogeneous domains. In general, when averaged over the entire C_{16} region, these samples show an overall average intensity decrease with increasing protein concentration. At a concentration of 0.1 mg/mL, an evenly distributed layer of protein is observed on the C_{16} SAM (Figure 8a). Increasing the concentration further led to a markedly uneven distribution of protein, suggesting aggregation and multilayer formation at the surface.

Assuming that the amount of adsorbed fibrinogen is proportional to the SEM grayscale intensity change, adsorption isotherm plots can be constructed to estimate a protein's equilibrium dissociation constant (K_D). This constant is the ratio of the product of the concentration of unbound protein [P] and surface sites [S] to that of surface adsorbed protein [P − S] at equilibrium (eq 6)

$$K_D = \frac{[P]\cdot[S]}{[P - S]} \tag{6}$$

and thus is an indication of the affinity a protein has toward a surface. The data in Figure 8b were fit using the functional form of a Langmuir isotherm (eq 7)

$$[B] = \frac{[F]\cdot B_{max}}{K_D + [F]} \tag{7}$$

where [B] and [F] are the concentration of bound fibrinogen and free fibrinogen in solution, respectively. The constants B_{max} and K_D indicate the percentage of binding sites bound and the equilibrium dissociation constant for fibrinogen on a C_{16} monolayer, respectively.[43] The extremely small K_D value ($\sim 10^{-9}$) is indicative of a protein that readily adsorbs to the hydrophobic SAM interface and is consistent with inferences developed using other forms of protein assays.[44−46] It should be noted, however, that the Langmuir model is almost certainly a gross oversimplification of the protein adsorption process, given the tendency of proteins to denature at the surface and in general behave nonideally.[47] Despite this, the experimental data are fit well by this simple model and provide a convenient indicator to numerically compare surface adsorption propensities.

The specific binding assay shown in Figure 9 provides a more direct verification of the quantitative bases of SE image contrasts. In this case, the strong binding of the biotin−avidin conjugate is directly imaged as contrast in the SEM grayscale. The image contrasts of the two pristine BSA monolayers are essentially indistinguishable, a result expected on the basis of the attenuation model. The binding of avidin, however, whose molecular weight is approximately equal to that of BSA (68 kDa), further attenuates the SE yield in a measurable way. Thus we see that the HDT regions show a noticeable attenuation of the intensity after the avidin exposure, indicating the adsorption of a ~12 Å thick protein layer in this region. The

(43) Chatelier, R. C.; Minton, A. P. *Biophys. J.* **1996**, *71*, 2367−2374.
(44) Chapman, R. G.; Ostuni, E.; Yan, L.; Whitesides, G. M. *Langmuir* **2000**, *16*, 6927−6936.
(45) Ta, T. C.; McDermott, M. T. *Anal. Chem.* **2000**, *72*, 2627−2634.
(46) Feldman, K.; Haehner, G.; Spencer, N. D.; Harder, P.; Grunze, M. *J. Am. Chem. Soc.* **1999**, *121*, 10134−10141.
(47) Lundstroem, I. *Phys. Scr.* **1983**, *T4*, 5−13.

BSA channel also darkens slightly, attenuated by the small degree of nonspecific adsorption occurring there. In stark contrast, the biotinylated-BSA channel shows significant attenuation, indicating the efficient formation of a higher mass coverage b-BSA/avidin conjugate. We conclude that simple extensions of this type of assay will allow the evaluation of more complex binding interactions while further enabling the rapid screening of large area assays with extremely high spatial resolution and sensitivity.

Conclusion

This work demonstrates the use of SEM as an analytical tool for detecting and quantifying both specific and nonspecific protein adsorption phenomena. Using SAMs on Au as a model system, the imaging mechanisms associated with this technique are shown, and a scalable method for quantification is proposed. The imaging mechanisms involved are universal and should be more generally applicable to studies of protein recognition using biomolecular arrays supported on other conductive substrates (such as silicon). In general terms, we expect that improvements in instrument design will also serve to extend the reach and utility of the procedures modeled here. The most difficult instrument related aspect of these experiments, which deserves specific comment, is the calibration of contrast and brightness settings, which on most modern instruments are highly automated parameters controlled by software not contemplating measurements of the type described here. Future instrument designs ideally would simplify the requirements for image calibration and expand the data range above the current 8bit digitization that limits the full range sensitivity of this method. Taken together, these improvements would allow a more direct approach to the quantitative imaging of protein adsorption on a surface.

Acknowledgment. This work was supported by the National Science Foundation (CHE0402420) and was carried at the Center for Microanalysis of Materials supported by the U.S. Department of Energy, Division of Materials Sciences under Award No. DEFG02-91-ER45439. The authors would like to gratefully acknowledge Dr. Jim Mabon and Dr. Rick Haasch for their technical assistance and useful discussion of SEM contrast mechanisms.

Supporting Information Available: Composite SEM image of self-assembled monolayers on Au; SEM micrograph of proteins adsorbed onto C16 arrays with no inert background SAMs; table of relevant data on proteins used in this work. This material is available free of charge via the Internet at http://pubs.acs.org.

JA060248+